https://doi.org/10.5194/egusphere-2024-707
Preprint. Discussion started: 15 March 2024

Revisiting the evolution of downhill thunderstorms over Beijing: A new perspective from radar wind profiler mesonet

Xiaoran Guo[a,b], Jianping Guo[a*], Tianmeng Chen[a], Ning Li[a], Fan Zhang[a], Yuping Sun[a],

[a]*State Key Laboratory of Severe Weather, Chinese Academy of Meteorological Sciences, Beijing 100081, China*

[b]*College of Earth and Planetary Sciences, University of Chinese Academy of Sciences, Beijing 100049, China*

Correspondence to:

Dr./Prof. Jianping Guo (Email: jpguo@cma.gov.cn; jpguocams@gmail.com)

https://doi.org/10.5194/egusphere-2024-707
Preprint. Discussion started: 15 March 2024

Abstract

Downhill thunderstorms frequently occur in Beijing during the rainy seasons, leading to substantial precipitation. The accurate intensity prediction of these events remains a challenge, partly attributed to insufficient observational studies that unveil the thermodynamic and dynamic structures along the vertical direction. This study provides a comprehensive methodology for identifying both enhanced and dissipated downhill thunderstorms. In addition, a radar wind profiler (RWP) mesonet has been built in Beijing to characterize the pre-storm environment downstream to the thunderstorms at the mountain foot. This involves deriving vertical distributions of high-resolution horizontal divergence and vertical motion from the horizontal wind profiles measured by the RWP mesonet. A case of enhanced downhill thunderstorm on 28 September 2018 is carried out, which support the idea that the enhanced southerly flow and corresponding convergence detected by the RWP mesonet could favorably support the development of thunderstorms in the afternoon. The results also indicate that low-level convergence is an effective signal in accounting for convective maintenance. Statistical analysis based on radar reflectivity from April to September 2018–2021 have shown that a total of 63 thunderstorm events tend to be enhanced after moving into downhill and urban areas, accounting for about 66 % of the total number of downhill thunderstorm events. A critical region for intensified thunderstorms lies on the downslope side of the mountains west to Beijing. The evolution of the downhill storm is associated with the dynamic conditions over the plain compared to its initial morphology. The lifting induced by stronger westerly winds and vertical shear in the low and midlevel troposphere exerts a critical influence on the enhancement of convection. The findings underscore the significant role of RWP network in elucidating the evolution of downhill storm.

https://doi.org/10.5194/egusphere-2024-707
Preprint. Discussion started: 15 March 2024

Short Summary

The prediction of downhill thunderstorm (DS) remains elusive due to the lack of profiling observations. Here we propose a novel objective method to identify the DS event and its evolutions, based on which enhance and dissipated DS are discriminated. The radar wind profiler (RWP) mesonet in Beijing is used to derive areal divergence and vertical velocity, which are used to explore the DS ambient environment. These dynamic variables from RWP help explain the spatio-temporal evolution of DS.

https://doi.org/10.5194/egusphere-2024-707
Preprint. Discussion started: 15 March 2024

1. Introduction

The complex evolution of convective systems crossing mountainous terrain represents a substantial forecasting challenge. It has been previously reported that downhill thunderstorms with intensive reflectivity and good organization are more likely to successfully maintain or strengthen compared to isolated and small-scale thunderstorms (Castro *et al.*, 1992). Various thermal factors that favor the development of downhill thunderstorm have been identified, including higher instability and lower convective inhibition (Letkewicz and Parker, 2010, 2011; Keighton *et al.*, 2007), adequate water vapor accompanied by low-level jets (Tompkins, 2001; McCaul and Cohen, 2004; Weckwerth *et al.*, 2014), and cool pool (Teng *et al.*, 2000; Jeevanjee and Romps, 2015; Li *et al.*, 2017; Xiao *et al.*, 2017). Furthermore, a few studies in the literature have demonstrated the importance of the dynamic environment over the plain, such as surface and low-tropospheric convergence for convection initiation (Frame and Markowski, 2006; Miglietta and Rotunno, 2009; Wilson *et al.*, 2010), and strong vertical wind shear (Parker *et al.*, 2007; Reeves and Lin, 2007; Xiao *et al.*, 2019).

The topography in Beijing is intricate, given its location at the foot of the Taihang Mountains to the west and the Yan Mountains to the north, both of which have ridges with elevations exceeding 1200 meters (Figure 1a). Wilson *et al.* (2007) found that downhill thunderstorms, particularly those originating from the west, constituted 79% of all thunderstorms in Beijing between 2003 and 2005, as determined through a statistical analysis of thunderstorm datasets. The distinctive topography and the frequent occurrence of downhill thunderstorm in Beijing afford us an excellent opportunity to observe the inherent dynamic structures of downhill thunderstorms and their pre-storm environments. This, in turn, allows for a more in-depth investigation into the potential physical mechanisms underlying the formation of this severe weather event. However, most of the previous studies are limited to the analysis of a single downhill thunderstorm case (Chen *et al.*, 2017; Sun and Cheng, 2017; Kang *et al.*, 2019). Besides, the investigation of pre-storm environment and evolution process of thunderstorm are either based on the model simulation (Chen *et al.*, 2005; Xiao *et al.*,

https://doi.org/10.5194/egusphere-2024-707
Preprint. Discussion started: 15 March 2024

2015; Li *et al.*, 2017) or reanalysis data (Wang *et al.*, 2019), largely owing to the dearth of high-density continuous vertical profiling measurements of wind, temperature, and humidity.

Furthermore, there exist no objective method that can be used to identify and track the propagation of downhill thunderstorm in the literature Therefore, more urgent efforts are warranted to investigate the difficult-to-forecast storm type from a statistical perspective of ground-based atmospheric profiling mesonet observations. A high-density mesonet, consisting of six radar wind profilers (RWP) has been established in the Beijing since 2018 (Figure 1b) to continuously observe three-dimensional wind fields with high temporal and vertical resolution. This provides us with a valuable tool to explore the atmospheric dynamic structures, such as areal averaged vorticity, divergence, and vertical velocity, of the pre-storm environment for the downhill thunderstorms by using the parameters derived from the RWP mesonet. The primary goals of this study are twofold: (1) to develop an objective method to identify the event of downhill thunderstorm and its evolution, mainly based on composite radar reflectivity from weather radar; and (2) to explore the statistical patterns of downhill thunderstorms and reveal the dynamical structures in the development of downhill thunderstorms, aiming to attain a deeper understanding of the evolution processes of these thunderstorms.

The next section describes the data and methodology, in which a novel objective method is proposed to characterize the evolution of downhill thunderstorm. Section 3 presents a case study of an enhanced downhill thunderstorm. Statistical analyses of the relationship is conducted in section 4 between wind profile, convergence and the evolution of downhill thunderstorms. A summary and concluding remarks are given in section 5.

https://doi.org/10.5194/egusphere-2024-707
Preprint. Discussion started: 15 March 2024

2. Methodology and data

2.1. Identification of downhill thunderstorms

To study the downhill thunderstorms in Beijing, areas in Figure 2a is selected as the region of interest (ROI). Then, ROI is divided into three subregions by terrain height: Area to the west and north of the ridge line is defined as the mountainous region (ROI_m), marking as dark gray in Fig. 2a; and the area with surface elevation less than 100 m is defined as the plain region (ROI_p), marked with white; the light-gray area between these two lines is defined as the downslope region (ROI_d).

The flow chart for identifying downhill thunderstorms from composite radar reflectivity is illustrated in Figure 2b, which is mainly comprised of the following steps: Firstly, based on the well-established findings in literature from previous studies (e.g., Kingsmill, 1995; Weckwerth, 2000; Qin and Chen, 2017; Bai *et al.*, 2019), echoes with radar reflectivity reaching over 35 dBZ triggered in ROI_m are identify as potential downhill thunderstorms. To eliminate false signals, those echoes with area less than 50 km^2 are filtered out.

Secondly, these potential clusters are tracked using the area overlapping method (Machado *et al.*, 1998; Huang *et al.*, 2018; Chen *et al.*, 2019). Noted that during merging processes, only the largest cluster is tracked continuously, while others are subsequently terminated. Likewise, during the splitting processes, only the largest cluster is tracked continuously, while others are attributed to newly initiated storms. Suppose the i^{th} (i = 1, 2, ...) thunderstorm (i.e., $\boldsymbol{S_i}$) is observed in ROI_m at time n (i.e., $\boldsymbol{T^n}$), the properties of S_i^n including the centroid (C_i^n), area (A_i^n) and maximum reflectivity (MR_i^n) are obtained.

Thirdly, the downhill thunderstorms are defined by whether the potential clusters move into ROI_d and ROI_p. And if the centroid of S_i crosses the ridge line and moves from ROI_m to ROI_d at time j, T^j is defined as the starting time when S_i begins to go down the hills. Similarly, if the centroid of S_i crossed the plain line and moves from

https://doi.org/10.5194/egusphere-2024-707
Preprint. Discussion started: 15 March 2024

ROI_d to ROI_p at time k, T^k is defined as the arrival time when S_i reaches the plain. Then, T^k-T^j is defined as the downhill duration of S_i. An example of S_i is depicted in Fig. 2a.

Finally, the downhill thunderstorms are classified into two categories, the enhanced downhill storms (EDS) and dissipated downhill storms (DDS). These two subsets are classified by comparing the area and maximum reflectivity at the time T^k to those at time T^j. If at least one of the criterions $A_i^k \geqq A_i^j$ and $MR_i^k \geqq MR_i^j$ fulfils, S_i is considered as an EDS, otherwise it is defined as a DDS.

2.2. Meteorological data

As depicted in section 2.1, radar reflectivity derived from the Doppler radar network dataset with a grid resolution of 0.01° at 10-min intervals during the rainy seasons (i.e., April−September) in 2018-2022 is used to identify downhill thunderstorms over Beijing.

Balloon soundings launched at the Zhangjiakou (ZJK) and Beijing Weather Observatory (BWO) (see their locations in Fig. 1b) are used to provide the vertical thermodynamic features during the downhill thunderstorms. The radiosonde launches twice a day at 0800, and 2000 Local Standard Time (LST), providing the vertical profiles of temperature, pressure, relative humidity, and horizontal winds with a vertical resolution of 5–8 m (Guo *et al.,* 2020).

Ground-based meteorological variables, including 2-m air temperature (T_{2m}), dew point temperature, and pressure measured at 5-min intervals and precipitation measured at 1-min intervals from automated surface stations (AWSs) are also used in the analysis over the study area.

Geopotential height at 500 hPa and horizontal wind at 850 hPa from the fifth generation ECMWF reanalysis (ERA5) datasets derived by European Centre for Medium-range Weather Forecasts (ECMWF) are used for analysing the large-scale conditions in a case study of a heavy precipitation event in Beijing. The dataset has 37 pressure levels, which is made publicly accessible on a grid spacing of 0.25° at hourly intervals (Hoffmann *et al.,* 2019).

https://doi.org/10.5194/egusphere-2024-707
Preprint. Discussion started: 15 March 2024

2.3. Radar wind profiler measurements

The RWP mesonet in Beijing, as presented in Table 1 and Fig. 1b, consists of six RWPs positioned at Shangdianzi (SDZ), Huairou (HR), Yanqing (YQ), Haidian (HD), Pinggu (PG), and BWO. The RWPs used in this study are CFL-6 Tropospheric Wind Profilers, manufactured by the 23rd Institute of China Aerospace Science and Industry Corporation. These instruments provide sampling height, horizontal wind direction and speed, vertical wind speed, horizontal credibility, vertical credibility, and refractive index structure parameter. And the data are recorded at 6-min intervals at 34 levels with a vertical resolution of 120 m below 4 km above the ground level (AGL) in low-operating mode, and at 25 levels with a vertical resolution of 240 m from 4 to 10 km AGL in high-operating mode (Liu *et al.*, 2019). Considering that the six RWPs located at different terrain heights, the horizontal velocities measured by each RWP are interpolated to the same altitude, starting from 0.5 km above mean sea level (AMSL) with a vertical resolution of 120 m.

Dynamic parameters, such as the horizontal divergence profiles can readily be calculated by vertical wind profile measurements derived from soundings or RWPs distributed along the perimeter of a circle or a triangle over an area (Bellamy, 1949; Carlson and Forbes, 1989; Lee *et al.*, 1995; Bony *et al.*, 2019). The reliability of the measurements and triangle method is demonstrated in the previous work (Guo *et al.*, 2023). Thus, we also employes this methodology to calculate the regional mean divergence, vorticity and vertical velocity profiles within the triangular regions built by the RWPs mesonet.

3. A case study of an EDS event

EDSs present significant challenges for local weather forecasters in accurately predicting the intensity of precipitation during nowcasting. In this section, an observational case study of this type of downhill thunderstorm is selected to explore the role of thermodynamic and dynamic environment on the evolution of the downhill thunderstorms.

https://doi.org/10.5194/egusphere-2024-707
Preprint. Discussion started: 15 March 2024

This storm originated from the ROI_m and began to go down the hill at 1200 LST of 28 September 2018, then hit Beijing after approximately 2–3 hours. Several AWSs in the Yanqing District recorded lightning activity and hails accompanied with an hourly rainfall amount of over 30 mm from 1430 to 1530 LST. It is noteworthy that the intensity of downhill thunderstorm became weakened before 1400 LST but intensified as it approached the plain area of Beijing.

3.1. Synoptic background

Sounding taken at the ZJK (Figure 3a) at 0800 LST located in the westerly flow sector, showed a surface-based temperature inversion below 900 hPa and a deep dry layer aloft from 850 hPa up to about 400 hPa. At the same time, similar temperature and humidity stratification was seen at the BWO (Figure 3b) with little convective available potential energy (CAPE) of 170.8 J kg^{-1} and convective inhibition (CIN) of 61 J kg^{-1}. The veering of a northwesterly wind to a westerly wind from 850 hPa to above 600 hPa indicated the presence of cold advection at 0800 LST. Even considering the possible enhancement of unstable layer as the mixed layer grew in the daytime, the thermal stratification seems insufficient to facilitate the initiation and subsequent organization of deep convection.

By contrast, larger-scale pre-storm environmental settings indicate favourable dynamic conditions for convective development during the passage of the downhill thunderstorm. At 500 hPa (Figure 3c), the large-scale conditions at 1400 LST on 28 Sep 2018 was characterized with a deep cold vortex at the border of Mongolia and China, and Beijing was situated in the cold sector, with a cold center approximately 500 km to the south, and influenced by strong westerly flows. At 850 hPa (Figure 3d), a trough extended from northeast to southwest over ROI_d, resulting in significant southwesterly flow prior to the trough over Beijing. The veering of a southwesterly wind at 850 hPa to a westerly wind 500 hPa indicated the presence of warm advection. The changeover from cold advection at 0800 LST to warm advection at 1400 LST in the lower troposphere could account for the subsequent deepening organization of convection after the thunderstorm entered the plain.

https://doi.org/10.5194/egusphere-2024-707
Preprint. Discussion started: 15 March 2024

3.2. Radar reflectivity and surface observations

Radar reflectivity at 1200 LST (Figure 4a) showed that a convective line with several convective cores was detected across the ridge line and moved gradually southeastward into ROI_d driven by the low-level northwesterly flows. Surface streamlines evidently showed dominant west-to-southwesterly surface winds in ROI_m and south-to-southwesterly flows in ROI_p (also see Figure 4a). In downslope regions, the local mountain-valley orientations appeared to account for up-valley flows in various directions. A surface analysis at 1200 LST, given in Figure 5a, shows a humid center in the northwest of the mountain region due to the previous precipitation, whereas the relative humidity of the downslope and plain was less than 60%. The thermal boundary near the ridge line which generated by the terrain could also be seen. T_{2m} over the plain area was on average of greater than 20 °C, whereas the mean T_{2m} over the mountainous region was less than 10°C. The large northwest-southeast-oriented temperature gradient appeared to account for the intensification and better organization of the at 1230 LST (Figure 5b). Surface convergence emerged ahead of the convective line, indicated by the streamlines in Figure 4b, which were associated with a pre-squall mesotrough/mesolow.

At 1300 LST, convective line with reflectivity exceeding 35 dBZ had spitted into two segments (Figure 4c). The northern segment was completely separated from the main storm in the southwest and then expanded northeastward by the intersecting streamlines, with another convective cell initiated near the local converging center around 117°E, 41.5°N before 1330 LST (Figure 4d). The southern segment maintained with the total rainfall exceeding 10 mm from 1300 to 1400 LST. In less than 30 minutes, cold downdrafts produced a sharp drop in T_{2m} by 6°C south of the convective cells (Figures 5c and d). Meanwhile, the wet center gradually moved eastward to the northeast of the mountain region (Figures 5c and d). Until 1400 LST, the convective cells started to merge into a linear convective system, and the frontal edge of the convection line had arrived triangle 1 with weaker intensity than before (Figure 4e). This could be closely associated with the relatively strong cold pool located in the south,

https://doi.org/10.5194/egusphere-2024-707
Preprint. Discussion started: 15 March 2024

which potentially cut off the warm southerly inflow from the plains to the mountains. Moreover, the cold-pool-induced horizontal vorticity could overpower the low-level wind shear, thereby facilitating the decreasing in radar reflectivity of the convection line (Rotunno *et al.,* 1988).

Composite radar reflectivity shows that a well-organized squall line was formed and propagated rapidly starting from 1400 LST (Figure 4e-4g). AWSs within triangle 1 captured its associated rainfall. Abrupt increase in surface pressure by +3 hPa was seen across the gust front in the triangle 1 when the maximum rainfall rate exceeded 3mm $(6\text{min})^{-1}$ (not shown). And the squall line intensified as it approaches ROI_p from 1400 to 1420 LST. This enhancement can potentially be attributed to the dynamic lifting over Beijing in terms of the inadequate moisture supply and instability. Due to the disadvantage of surface observations in monitoring the vertical dynamic features, the evolution of high-resolution divergence and vertical velocity derived from the RWP mesonet will be further explored.

3.3. Divergence and vertical velocity

Before the convective system reach the plain area, sustained southwesterly wind above 2 km AMSL is observed after 1200 LST at YQ station (Figure 6a), accompanied with upper-layer divergence and downdraft in triangle 1 (Figure 6b), which was likely driven by downslope flows from the western mountains. The much weaker near-surface southerly wind and divergence could to a certain extent be influenced by the valley flows at the foot of the mountains. Meanwhile, a peak of positive vorticity exceeding 10^{-4} s^{-1} and a deep layer of negative vorticity up to 5 km AMSL in triangle 1 were maintained during this time period (Figure 6c). Then, pronounced southerly wind occurred after 1300 LST that corresponded to the rapidly intensification in convergence below 2 km, providing an uplifting background, albeit less than 0.1 m s^{-1}. This updraft assisted the upward transport of moist air in the planetary boundary layer (PBL), which facilitated the subsequent formation of clouds and convective rainfall. Additionally, a vorticity maximum near 3×10^{-4} s^{-1} at 1348 LST in the PBL may also be favorable for organized convective development.

https://doi.org/10.5194/egusphere-2024-707
Preprint. Discussion started: 15 March 2024

At 1412 LST, wind speed below 1.5 km AMSL is weaker than 5 m s^{-1} while is stronger than 15 m s^{-1} above 2.5 km AMSL. The low-level wind speeds over YQ started to increase to 10 m s^{-1} because of the downward momentum transport. The subsequent increase in convergence coincided well with the intensification of southwesterly winds (>10 m · s^{-1}) up to 3 km ASML after 1418 LST. Such intensification in convergence and updraft were also well captured by triangles 2 (not shown), even with more than one hour in advance of the convective rainfall arrival. Upward motion in triangle 1 increase in amplitude and deepen rapidly in depth as the squall line propagated southeastward, and triggered rainfall over triangle 1. The most intense convergence occurred at 1430 LST and extended from 1 km to above 2.5 km AMSL afterwards as a result of latent heat release during cloud formation. The maximum vertical velocity reached 0.35 m s^{-1} around 3.5 km AMSL, which were about 6 min prior to the peak area-averaged rainfall rate at 1448 LST. The significant convergence diminished after 1454 LST, when deep convection moved out of triangle 1. Downdrafts are found with moderate upward and downward motions in the stratiform area. Clearly, this result can help understand the propagation and intensity evolution of the thunderstorm.

4. Statistical results

4.1. General features of downhill thunderstorm events

To obtain a more robust understanding of the climatology for downhill thunderstorm evolution in Beijing, an in-depth statistical analysis is carried out in this study. According to the methodology mentioned in Section 2.1, we firstly identified a total number of 95 downhill thunderstorms triggered in ROI_m and moved into ROI_d and ROI_p in the study area (Figure 1b) based on the radar reflectivity datasets during the rainy seasons (i.e., April- September) in 2018-2022.We perform a statistical analysis of the occurrence number of radar reflectivity that is equal to or greater than 35 dBZ on a grid spacing of 0.01° at 10-min intervals during these downhill thunderstorm events.

As shown in Figure 7a, downhill thunderstorms tend to occur and develop in ROI_d with strong steep slopes rather than northern mountainous area at higher altitudes. The

https://doi.org/10.5194/egusphere-2024-707
Preprint. Discussion started: 15 March 2024

high-frequency center is found mainly over the western downhill area with the occurrence number exceeding 400, due possibly to the large amount of eastward propagation of thunderstorms driven by the westerly or southwesterly flows during the warm seasons in Beijing (Chen *et al.*, 2012, 2014).

For all downhill thunderstorms, the relationship between the initial area and length-width ratio of thunderstorms at the beginning and the relative variation of area to the time it arrives ROI_p is analyzed. Here, we record the maximum (minimum) axis length of the radar echo with reflectivity ≥35 dBZ as the length (width) of the downhill thunderstorm, respectively. The area and length-width ratio tends to reflect the horizontal scale and organization of convective storms. Generally, linear convective storms show a length-width ratio greater than or equal to 3.0 (Chen and Chou, 1993; Meng *et al.*, 2013; Yang *et al.*, 2017). The results show that several mature thunderstorms with the area larger than 5000 km^2 tend to dissipate during the downhill process with weaker intensity and area, which are likely due to the splitting processes (Figure 7b). Convective lines commonly intensify to the squall lines, but several isolated and loose thunderstorms expand rapidly during the downhill process with increasing area when enter the plain, which may be associated with the favorable regional-scale lower tropospheric environment.

It is found that 63 thunderstorms events tend to be enhanced after it moved into the downhill and urban areas, accounting for about 66 % of the total number of downhill thunderstorms events, whereas 32 thunderstorm events tend to be dissipated. Most of the downhill thunderstorms arrive the plain area in early mornings and late afternoons (Figure 7c). And the occurrence of DDS is much less than EDS. At 0100-0800 LST, the DDS events accounts for 8% of all downhill storms during this period, and the percentage of DDS events is still much smaller than that of the EDS events during the period of 1400-0000 LST, although reaching 15%. The thunderstorms from the west basically take about two hours to go down the hill while those from the northwest and north take a longer time possibly due to the further distance.

https://doi.org/10.5194/egusphere-2024-707
Preprint. Discussion started: 15 March 2024

4.2. Dynamic conditions

To better understand the similarities and differences between EDS and DDS from the perspective of ambient atmospheric environment, three-dimensional dynamic structures derived from RWP mesonet are analyzed. Variables including wind speed, vertical wind shear, u-component and v-component of wind, divergence and vorticity profiles are used to provide information of dynamic structures before the downhill thunderstorms arrive. Since the western part of ROI_d is a key area for the development of downhill thunderstorms (Figure 7a), we focus on these parameters from YQ station and triangle 1 in the following discussions.

The mean vertical wind profiles two hours prior to the arrival of the thunderstorms are investigated. Horizontal wind speed, vertical wind shear, u- and v-component from the RWP in YQ, and divergence and vorticity over triangle 1 are calculated (Figure 8). Results indicate that wind speed and vertical wind shear (VWS) below 1.5 km AMSL have small differences between EDSs and DDSs before their arrival (Figure 8a, b). But much stronger horizontal winds and VWS are observed in the 1.5-5 km layer in advance of the EDS events, which could be likely associated the critical influence that high vertical wind shear exerts on convection. Notably, the EDSs mainly appears within 5 km AMSL as the strong westerly winds prevails (Figure 8c), which well corroborates the results from Figure 7b. The downhill storms seem mainly dominated by the southerly component of winds in the lowest 2.5 km layer (Figure 8d). But for EDS events, v-component of wind are stronger below 2.5 km AMSL and near-zero above 3 km AMSL. This can be associated with the stronger up-valley flows during EDS events, which may possibly allow for stronger upward transport of water vapor and lead to intensifications of thunderstorms. The southerly component of winds before DDS events increases with altitude but remains much weaker than the westerly component. The presence of warm advection induced by the veering of a southwesterly wind at low level to a midlevel westerly wind may provide a favorable regional environment for the subsequent deepening organization of EDSs.

https://doi.org/10.5194/egusphere-2024-707
Preprint. Discussion started: 15 March 2024

The mean vertical structure of divergence and vorticity are given in Figure 8e and f. Compared with DDSs, the near-surface convergence is more evident near the arrival of EDSs, cooperating with the upward motion over the plain (figure 8b). The lifting may contribute to closer coupling between boundary layer and clouds, especially when instability and moisture supply are unfavorable. The vorticity field in figure 8f is characterized by cyclonic flows at lower-levels and anticyclonic flows at midlevel, which is possibly dependent on the synoptic forcing. The cooperation between lower-level cyclones and convergence tends to promote the maintenance of updrafts, leading to heavy rainfall. But the vorticity prior to EDSs seems to be weaker than that of DDSs, this difference may be associated with the mountain-valley wind breeze. Also, the stronger winds at 2-3 km shown in figure 8a may trigger meso-scale circulations and induce vorticity disturbances. This interaction between mountain morphology, urban effects, and dynamic structure is complex, which needs to be explored in the future.

5. Summary and concluding remarks

Given the large uncertainty in prediction and huge impact, here we revisited the evolution of downhill thunderstorms and concurrent ambient atmospheric dynamic structures as derived from a high-density radar wind profiler (RWP) mesonet in Beijing. This RWP mesonet in Beijing is shown to be capable of continuously observing the horizontal wind fields in the lower troposphere with ultra-high vertical and temporal resolutions. It follows that the profiles of vertical wind shear, divergence and vorticity are derived from the triangle algorithm, which are used to analyze the pre-storm dynamic environment for the downhill storms.

First of all, a novel objective methodology has been developed to identify and track the downhill thunderstorms. Combined with the changes in size or intensity of radar echoes, enhanced downhill thunderstorms (EDSs) and dissipated downhill thunderstorms (DDSs) are discriminated. A case study of an EDS during the period of 1200-1500 LST of 28 September 2018 is performed. Of interest is that the intensity of downhill thunderstorm became weakened before 1400 LST but intensified as it

https://doi.org/10.5194/egusphere-2024-707
Preprint. Discussion started: 15 March 2024

approached the plain area of Beijing. The synoptic background shows the presence of unfavorable thermodynamic conditions with small CAPE and inadequate water vapor supply. The enhanced southerly flow in the lower troposphere and the corresponding convergence detected by the RWP mesonet, together with automated weather observations, could favorably support the deepening organization of convection.

To obtain a robust result concerning the evolution characteristics of the downhill thunderstorms in Beijing, an in-depth statistical analysis is merited. The beginning and arrival time of a downhill thunderstorm event are defined as the moment when the centroid crosses the ridge line and plain, respectively. A total of 95 downhill thunderstorms events occurring in the study area are identified based on the datasets of radar reflectivity at 10-min intervals during the rainy season (i.e., April- September) of 2018–2022. The high occurrence frequency center of convection is found mainly resides west to Beijing' plain area. And the area variation of convection is not sensitive to the initial morphology itself. It is found that 63 thunderstorms tend to be enhanced with larger area or radar reflectivity after it moved into the downhill and urban areas, accounting for about 66 %. The statistical analysis indicates that most of the downhill thunderstorms affect the plains around 0400 and after 1600 LST. Most downhill processes last about two hours while thunderstorms from the northwest and the north may take a longer time possibly due to the further distance.

Thus, we illustrate the statistical analysis of dynamic quantities, such as horizontal winds, vertical wind shears derived from the RWP at the mountain foot, and divergence and vorticity derived from the west-most triangular region in the RWP mesonet, in relation to the enhanced and dissipated downhill storms. Results indicate that much stronger horizontal winds and vertical wind shear are observed in 1.5-5 km layer in advance of the EDS events and exert a critical influence on the development of storms. Furthermore, the presence of warm advection induced by the veering of a southwesterly wind at low level to a midlevel westerly wind provide a favorable regional environment for the subsequent deepening organization of convection. The lower-level convergence and cyclonic flows over the plain contribute to the development of robust updrafts and

https://doi.org/10.5194/egusphere-2024-707
Preprint. Discussion started: 15 March 2024

closer coupling between boundary layer and clouds, which favors the intensification of downhill thunderstorms.

Continuous measurements of the accurate dynamic quantities will make it possible to enable a more critical and quantitative evaluation for the development of downhill thunderstorms in the future. It should be noted that we have merely analyzed the roles of dynamic features derived from the RWP mesonet in determining the uplifting. However, wind field and convergence are not the only variables that determine the enhancement or dissipation of downhill storms. In further study, statistics analysis of some thermodynamic parameters, such as CAPE, K index, precipitable water, will be performed to characterize the pre-storm environments in detail.

Data Availability

We are grateful to ECMWF for providing ERA5 hourly data (https://www.ecmwf.int/en/forecasts/datasets/reanalysis-datasets/era5/). The radar wind profiler data are obtained from the National Meteorological Information Center of China Meteorological Administration (https://data.cma.cn), which can be only accessed via registration.

Acknowledgments

This work was supported by the National Natural Science Foundation of China under Grants of 42325501, U2142209 and 42105090. Last but not least, we appreciated tremendously the constructive comments and suggestions made by the anonymous reviewers that significantly improved the quality of our manuscript.

Author Contributions

The study was completed with close cooperation between all authors. JG designed the research framework; XG performed the analysis and drafted the original manuscript with contribution from JG; JG, TC, NL, FZ and YS helped revise the manuscript.

Completing interests

The authors declare that they have no conflict of interest.

https://doi.org/10.5194/egusphere-2024-707
Preprint. Discussion started: 15 March 2024

References

Bai, L., Meng, Z., Huang, Y., Zhang, Y., Niu, S., and Su, T., 2019: Convection initiation resulting from the interaction between a quasi‐stationary dryline and intersecting gust fronts: A case study. *Journal of Geophysical Research: Atmospheres*, 124, 2379–2396. https://doi.org/10.1029/2018JD029832.

Bellamy, J.C. (1949) Objective calculations of divergence, vertical velocity and vorticity. *Bulletin of the American Meteorological Society*, 30, 45-49, https://doi.org/10.1175/1520-0477-30.2.45.

Bony, S., and B. Stevens, 2019. Measuring area-averaged vertical motions with dropsondes. *Journal of the Atmospheric Sciences*, 76,767-783, doi: 10.1175/JAS-D-18-0141.1.

Carlson C.A., and G.S. Forbes, 1989. A case study using kinematic quantities derived from a triangle of VHF Doppler Wind Profilers. *Journal of Atmospheric and Oceanic Technology*, 6, 769-778, doi: 10.1175/1520-0426(1989)006<0767:ACSUKQ>2.0.CO;2.

Castro A, Sánchez J. L., Fraile R., 1992: Statistical comparison of the properties of thunderstorms in different areas around the Ebro-Valley (Spain). *Atmospheric Research*, 28(3-4): 237-257, doi: 10.1016/0169-8095(92)90011-x.

Chen, D., J. Guo, D. Yao, and Coauthors, 2019: Mesoscale convective systems in the Asian monsoon region from Advanced Himawari Imager: Algorithms and preliminary results. *Journal of Geophysical Research: Atmospheres*, 124, 2210-2234, doi: 10.1029/2018JD029707.

Chen G. T.-J., and H.-C. Chou, 1993: General characteristics of squall lines observed in TAMEX. *Monthly Weather Review*, 121, 726–733.

Chen M., Y. Wang, F. Gao, et al., 2012: Diurnal variations in convective storm activity over contiguous North China during the warm season based on radar mosaic climatology. *Journal of Geophysical Research: Atmospheres*, 117(D20).

Chen M., Y. Wang, F. Gao, et al., 2014: Diurnal evolution and distribution of warm-season convective storms in different prevailing wind regimes over contiguous North China. *Journal of Geophysical Research: Atmospheres*, 119(6): 2742-2763.

Chen M., X. Xiao, F. Gao, et al., 2017: Dynamical effect of outflow boundary on localized initiation and rapid enhancement of severe convection over Beijing–Tianjin–Hebei region. *Chinese Journal of Atmospheric Sciences (in Chinese)*, 41 (5): 897–917, doi: 10.3878/j.issn.1006-9895.1702.16101.

Chen S.-H. and Y.-L. Lin, 2005: Effects of moist Froude number and CAPE on a conditionally unstable flow over a mesoscale mountain ridge. *Journal of Atmospheric Sciences*, 62, 331–350.

Chu C.-M. and Y.-L. Lin, 2000: Effects of orography on the generation and propagation of mesoscale convective systems in a two-dimensionally conditionally unstable flow. *Journal of Atmospheric Sciences*, 57, 3817–3837.

Feng, Z., R. A. Houze, Jr., L. R. Leung, F. Song, J. C. Hardin, J. Wang, W. I. Gustafson, Jr., and C. R. Homeyer, 2019: Spatiotemporal characteristics and large-scale environments of mesoscale convective systems east of the Rocky Mountains. *Journal of Climate*, 32, 7303–7328.

Frame, J. W., and P. Markowski, 2006: The interaction of simulated squall lines with idealized mountain ridges. *Monthly Weather Review*, 134, 1919–1941, https://doi.org/10.1175/MWR3157.1.

Guo, J., X. Chen, T. Su, and Coauthors (2020) The climatology of lower tropospheric temperature inversions in China from radiosonde measurements: roles of black carbon, local meteorology, and large-scale subsidence. *Journal of Climate*, 33, 9327–9350, https://doi.org/10.1175/JCLI-D-19-0278.1.

Guo, X., Guo, J., Zhang, D-L., & Yun, X., 2023: Vertical divergence profiles as detected by two wind profiler mesonets over East China: implications for nowcasting convective storms, *Quarterly Journal of the Royal Meteorological Society*, doi:10.1002/qj.4474.

https://doi.org/10.5194/egusphere-2024-707
Preprint. Discussion started: 15 March 2024

Hoffmann, L., Günther, G., Li, D., Stein, O., Wu, X., Griessbach, S., Heng, Y., Konopka, P., Müller, R., Vogel, B., and Wright, J. S., 2019. From ERA-Interim to ERA5: the considerable impact of ECMWF's next-generation reanalysis on Lagrangian transport simulations. *Atmospheric Chemistry and Phys*ics, 19, 3097–3124, https://doi.org/10.5194/acp-19-3097-2019.

Huang, X. M., Hu, C. Q., Huang, X., Chu, Y., Tseng, Y., Zhang, G. J., & Lin, Y. L., 2018: A long-term tropical mesoscale convective systems dataset based on a novel objective automatic tracking algorithm. *Climate Dynamics*, 51, 3145–3159. https://doi.org/10.1007/s00382-018-4071-0

Jeevanjee, N., and D. M. Romps, 2015: Effective buoyancy, inertial pressure, and the mechanical generation of boundary layer mass flux by cold pools. *Journal of Atmospheric Sciences*, 72, 3199–3213.

Kang Y., X. Peng, S. Wang, Y. Hu, and S. Lu, 2019: Observational analyses of topographic effects on convective systems in an extreme rainfall event in northern China. *Atmospheric Research*, 229, doi: 10.1016/j.atmosres.2019.05.024.

Keighton, S., J. Jackson, J. Guyer, and J. Peters., 2007: A preliminary analysis of severe quasi-linear mesoscale convective systems crossing the Appalachians. Preprints, 22nd Conf. on Weather Analysis and Forecasting, Park City, UT, *American Meteorological Society*, P2.18.

Kingsmill, D. E., 1995: Convection initiation associated with a sea-breeze front, a gust front, and their collision. *Monthly Weather Review*, 123, 2913–2933.

Lee, J.L., G.L. Browning, and Y.F. Xie (1995) Estimating divergence and vorticity from the wind profiler network hourly wind measurements. *Tellus Series A-dynamic Meteorology & Oceanography*, **47**, 892-910, https://doi.org/10.1034/j.1600-0870.1995.00127.x.

https://doi.org/10.5194/egusphere-2024-707
Preprint. Discussion started: 15 March 2024

Letkewicz C. E. and M. D. Parker, 2011: Impact of environmental variations on simulated squall lines interacting with terrain. *Monthly Weather Review*, 139(10): 3163-3183.

Letkewicz C. E. and M. D. Parker, 2010: Forecasting the maintenance of mesoscale convective systems crossing the Appalachian Mountains. *Weather and Forecasting*, 25, 1179–1195.

Li, H., X. Cui, and D. Zhang, 2017: On the initiation of an isolated heavy-rain-producing storm near the central urban area of Beijing metropolitan region. *Monthly Weather Review*, 145, 181–197, https://doi.org/10.1175/MWR-D-16-0115.1.

Liu, B., Y. Ma, J. Guo, W. Gong, Y. Zhang, J. Li, X. Guo, and Y. Shi, 2019: Boundary layer heights as derived from ground-based radar wind profiler in Beijing, *IEEE Transactions on Geoscience and Remote Sensing*, 57(10), 8095-8104, doi: 10.1109/TGRS.2019.2918301.

Machado, L. A. T., Rossow, W. B., Guedes, R. L., & Walker, A. W., 1998: Life cycle variations of mesoscale convective systems over the Americas. *Monthly Weather Review*, 126, 1630–1654. https://doi.org/10.1175/15200493(1998)126<1630:LCVOMC>2.0.CO;2

McCaul, E. W., Jr., and C. Cohen, 2004: The initiation, longevity and morphology of simulated convective storms as a function of free tropospheric relative humidity. Preprints, 22nd Conf. on Severe Local Storms, Hyannis, MA, *American Meteorological Society*, 8A.5.

Meng Z., D. Yan, and Y. Zhang, 2013: General features of squall lines in East China. *Monthly Weather Review*,141(5), 1629-1647, doi:10.1175/MWR-D-12-00208.1.

Miglietta, M. M., and R. Rotunno, 2009: Numerical simulations of conditionally unstable flows over a mountain ridge. *Journal of Atmospheric Sciences*, 66, 1865–1885.

https://doi.org/10.5194/egusphere-2024-707
Preprint. Discussion started: 15 March 2024

Parker, M. D. and R. H. Johnson, 2004: Simulated convective lines with leading precipitation. Part I: Governing dynamics. *Journal of Atmospheric Sciences*, 61, 1637–1655.

Parker, M. D. and D. A. Ahijevych, 2007: Convective episodes in the east-central United States. *Monthly Weather Review*, 135, 3707–3727.

Qin, R., and M. Chen, 2017: Impact of a front–dryline merger on convection initiation near a mountain ridge in Beijing. *Monthly Weather Review*, 145, 2611-2633, doi: 10.1175/MWR-D-16-0369.1.

Reeves, H. D. and Y.-L. Lin, 2007: The effects of a mountain on the propagation of a preexisting convective system for blocked and unblocked flow regimes. *Journal of Atmospheric Sciences*, 64, 2401–2421.

Rotunno, R., J. B. Klemp, and M. L. Weisman, 1988: A theory for strong, long-lived squall lines. *Journal of Atmospheric Sciences*, 45, 463–485.

Sun J., Cheng G., 2017: Influence of thermal and dynamical conditions over Beijing city area on strength of down-to-hill thunderstorms. *Plateau Meteorology*, 36(1): 207–218, doi:10.7522/j.issn.1000-0534.2016.00007.

Teng, J.-H., C.-S. Chen, T.-C. C. Wang, and Y.-L. Chen, 2000: Orographic effects on a squall line system over Taiwan. *Monthly Weather Review*, 128, 1123–1138, https://doi.org/10.1175/1520-0493(2000)128<1123:OEOASL>2.0.CO;2.

Tompkins, A. M., 2001: Organization of tropical convection in low vertical wind shears: The role of water vapor. *Journal of Atmospheric Sciences*, 58, 529–545, https://doi.org/10.1175/1520-0469(2001)058<0529:OOTCIL>2.0.CO;2.

Wang J., M. Zhang, S. Ren, et al., 2019: Simulation study on the impact of Taihang Mountain slopes on down hill front cyclone rainstorm. Advances in Earth Science, 34(7), 717-730, doi: 10.11867/j.issn.1001-8166.2019.07.0717.

Weckwerth, T. M., 2000: The effect of small-scale moisture variability on thunderstorm initiation. *Monthly Weather Review*, 128, 4017–4030.

Weckwerth T M, Bennett L J, Miller L J, et al., 2014: An observational and modeling study of the processes leading to deep, moist convection in complex terrain. *Monthly Weather Review*, 142(8): 2687-2708.

Wilson J. W., Chen M. X., Wang Y. C., 2007: Nowcasting thunderstorms for the 2008 summer Olympics. The 33rd International Conference on radar Meteorology. Cairns: Australia, *American Meteorological Society*, 12.

Wilson J. W., Feng Y., Chen M., et al., 2010: Nowcasting challenges during the Beijing Olympics: Successes, failures, and implications for future nowcasting systems. *Weather and Forecasting*, 25, 1691-1714, doi: 10.1175/2010WAF2222417.1.

Xiao X., M. Chen, F. Gao, et al., 2015: A thermodynamic mechanism analysis on enhancement or dissipation of convective systems from the mountains under weak synoptic forcing. *Chinese Journal of Atmospheric Sciences (in Chinese)*, 39 (1): 100–124.

Xiao X, Sun J, Chen M, et al., 2017: The characteristics of weakly forced mountain ‐ to ‐ plain precipitation systems based on radar observations and high ‐ resolution reanalysis. *Journal of Geophysical Research: Atmospheres*, 2017, 122(6): 3193–3213.

Xiao X, Sun J, Chen M, et al., 2019: Comparison of environmental and mesoscale characteristics of two types of mountain ‐ to ‐ plain precipitation systems in the Beijing region, China. *Journal of Geophysical Research: Atmospheres*, 2019, 124(13): 6856-6872.

Yang X. L., Sun J. H., Zheng Y. G., 2017: A 5-yr climatology of severe convective wind events over China. *Weather and Forecasting*, 32(4), 1289-1299, doi:10.1175/WAF-D-16-0101.1.

https://doi.org/10.5194/egusphere-2024-707
Preprint. Discussion started: 15 March 2024

Table 1. Summary of six radar wind profilers in Beijing.

Station Name	Acronym	Lat. (°N)	Lon. (°E)	Alt. (m, AMSL)
Shangdianzi	SDZ	40.66	117.11	286.5
Huairou	HR	40.36	116.63	75.6
Yanqing	YQ	40.45	115.97	489.4
Haidian	HD	39.98	116.28	46.9
Pinggu	PG	40.17	117.12	32.1
Beijing Weather Observatory	BWO	39.79	116.47	32.5

https://doi.org/10.5194/egusphere-2024-707
Preprint. Discussion started: 15 March 2024

Figures

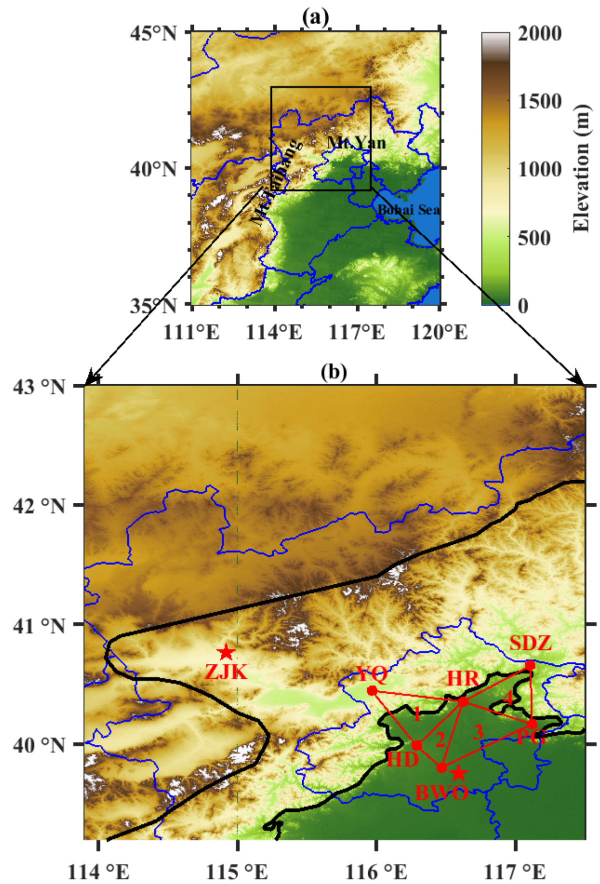

Figure 1. (a) Spatial distribution of the topography over northern China with the blue line denoting the Province boundaries. The locations of Taihang Mountains (Mt. Taihang), Yan Mountains (Mt. Yan) and Bohai Sea are written in black text. (b) Map of Beijing with six RWPs (red dots) deployed at Shangdianzi (SDZ), Huairou (HR), Yanqing (YQ), Haidian (HD), Pinggu (PG), and the Beijing Weather Observatory (BWO) and surrounding areas. The BWO and Zhangjiakou (ZJK) are deployed with an L-band radiosonde (red pentagrams). The four red triangles denote the areas used to calculate the horizontal divergence with the triangle method. The left black line mark the ridge line, and the right black line mark the plain line that denotes the 200-m terrain elevation.

https://doi.org/10.5194/egusphere-2024-707
Preprint. Discussion started: 15 March 2024

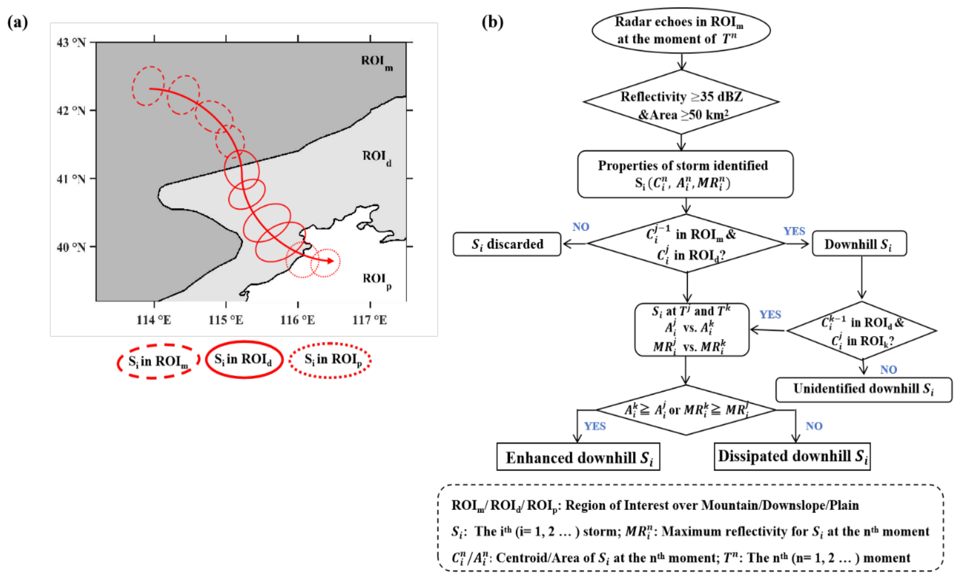

Figure 2. (a) Definition of the ROIs and the schematic diagram showing the track of a downhill thunderstorm S_i (red circle). The red arrow denotes the trajectory of S_i. (b) Flow chart showing the primary processes to identify downhill thunderstorms in this study.

https://doi.org/10.5194/egusphere-2024-707
Preprint. Discussion started: 15 March 2024

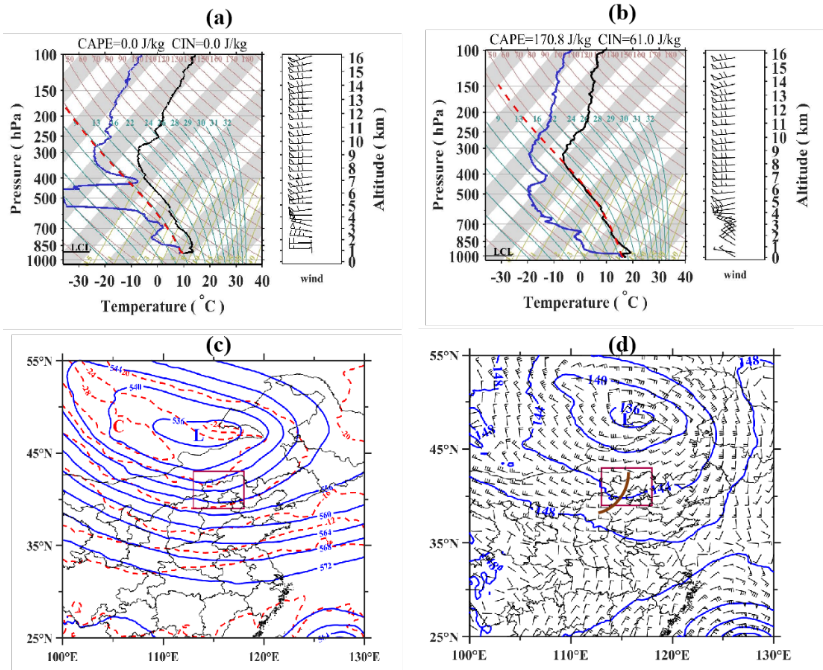

Figure 3. (a) SkewT/Log P diagram of upper-air sounding at the ZJK at 0800 LST of 28 Sep 2018 (a full barb is 4 m s^{-1}). (b) Same as (a) but for the upper-air sounding at the BWO. (c) Horizontal distribution of geopotential height at 500 hPa (solid blue lines at 40 gpm intervals) and temperature (dashed red lines at intervals of 4° C) at 1400 LST of 28 Sep 2018, which are both obtained from the ERA5 hourly reanalysis data. The purple rectangle indicates the location of the study area shown in Figure 1b. Letters "L" and "C" denote the centers of a low-pressure system, and cold air, respectively. (d) Same as (c), but for geopotential height at 850 hPa (solid blue lines at 40 gpm intervals) and horizontal wind vectors at 850 hPa (m s^{-1}). Note the distribution of a trough along the thick brown line.

https://doi.org/10.5194/egusphere-2024-707
Preprint. Discussion started: 15 March 2024

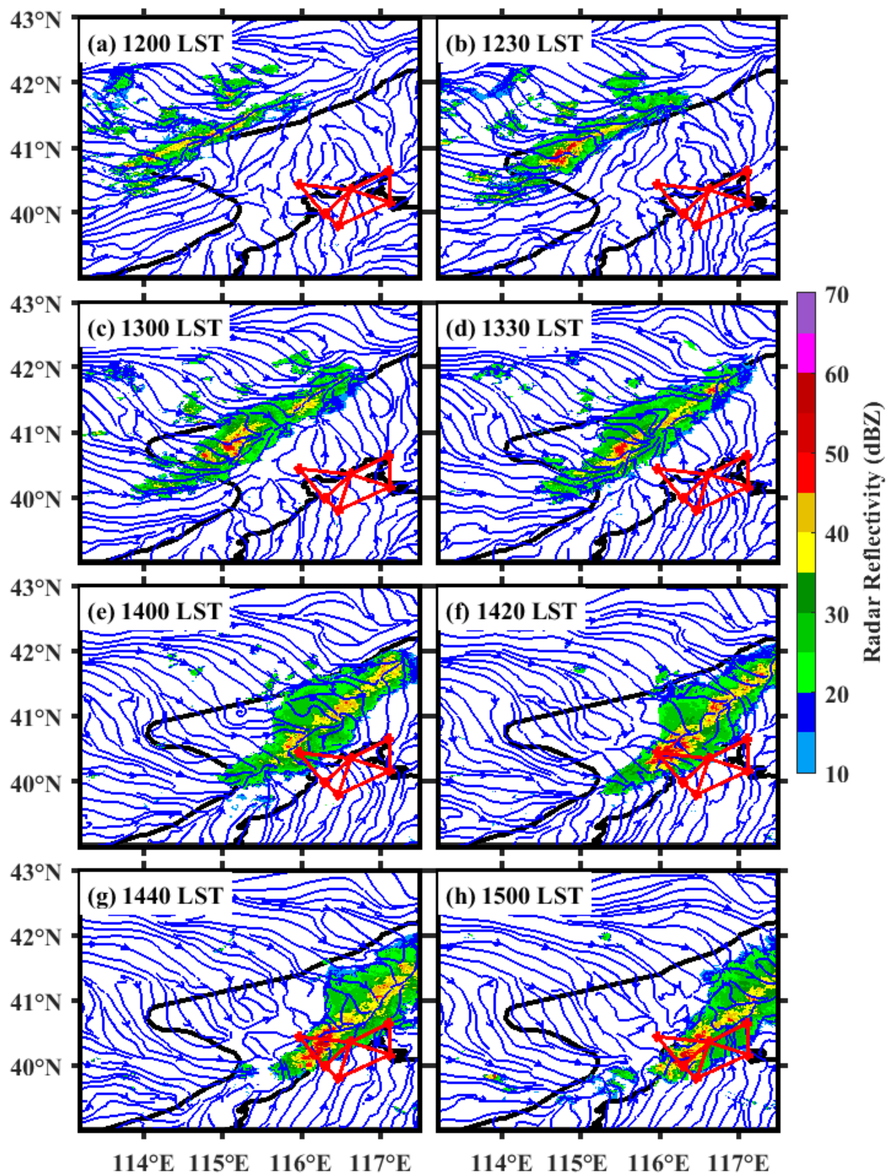

Figure 4. Evolution of the radar reflectivity (color-shaded, dBZ) and surface streamlines derived from AWSs from (a) 1200 to (h) 1500 LST 28 September 2018. The four red triangles denote the regions used to calculate the horizontal divergence and vertical motion with the triangle method. The two black lines mark the boundaries of the ROI_m, ROI_d and ROI_p.

https://doi.org/10.5194/egusphere-2024-707
Preprint. Discussion started: 15 March 2024

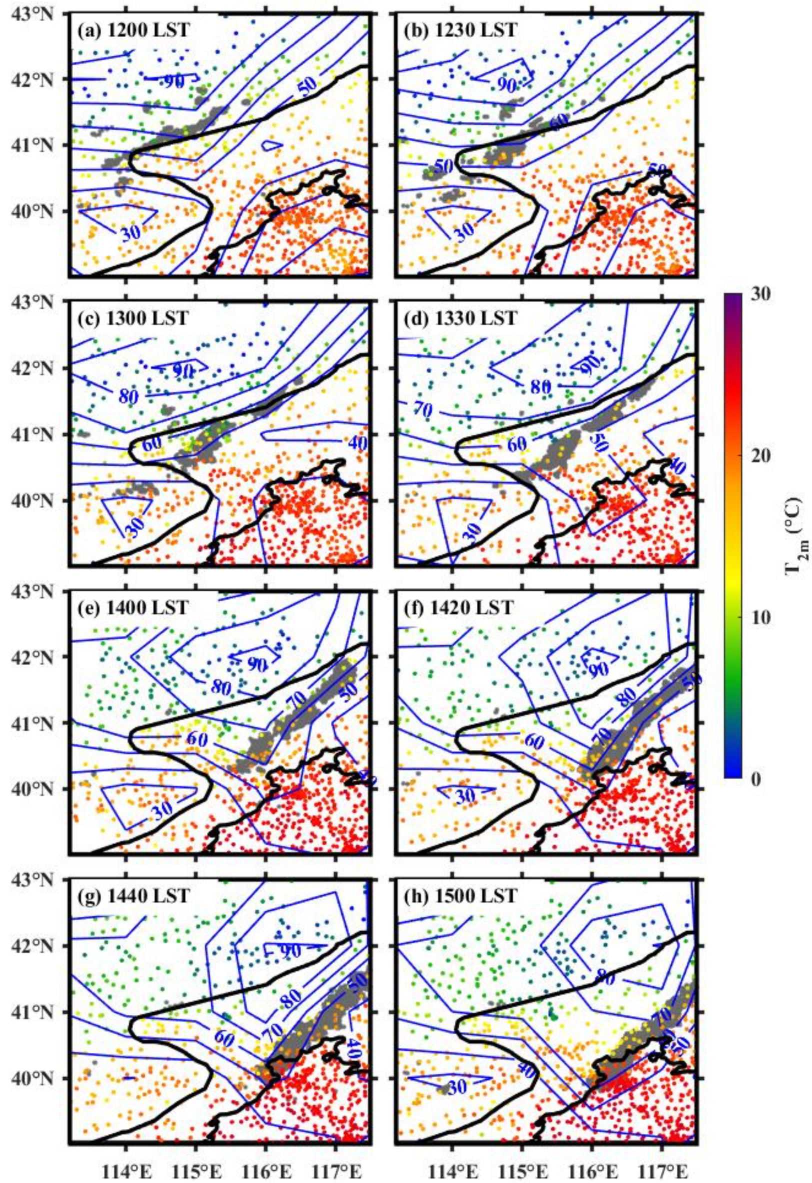

Figure 5. Evolution of the T_{2m} (color-shaded, °C) and relative humidity (contour, %) derived from AWSs from (a) 1200 to (h) 1500 LST 28 Sep 2018. The left black line is the ridge line, the right black line is the plain line which denotes the 200-m terrain elevation. The gray region denotes the position of echo with radar reflectivity exceeding 35 dBZ.

https://doi.org/10.5194/egusphere-2024-707
Preprint. Discussion started: 15 March 2024

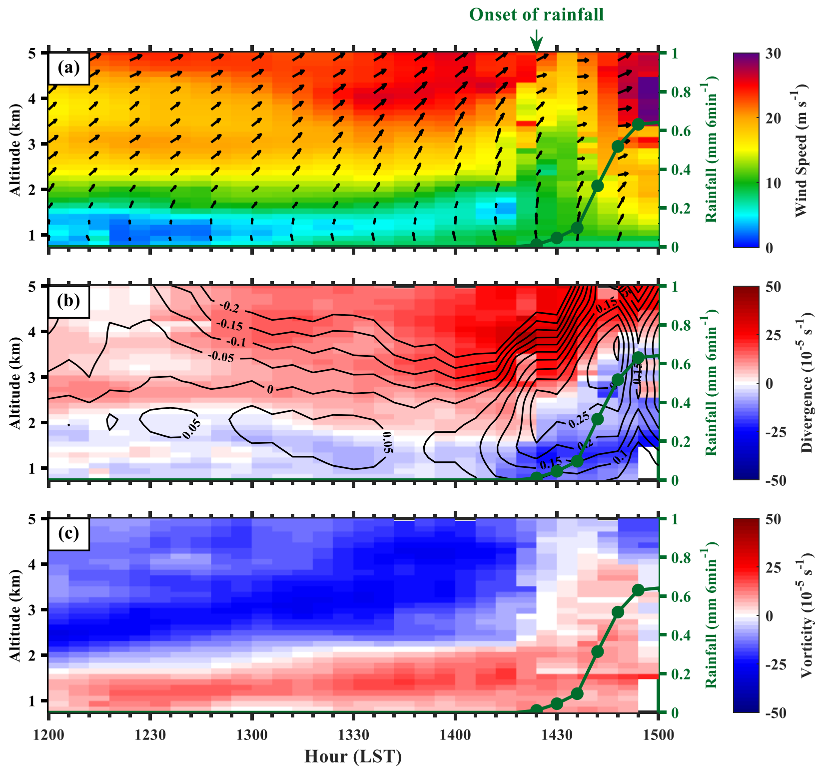

Figure 6. (a) Time series of horizontal wind vectors (m · s^{-1}) with wind speeds shaded in the 0.5–5-km AMSL layer during the period of 1200-1500 LST 28 Sep 2018 at YQ station. Green-dotted lines represent the triangle-area-averaged rainfall amount (mm 6min^{-1}) of triangle 1. (b) same as (a), but for the vertical profiles of the triangle-averaged divergence (shaded, 10^{-5} s^{-1}) and vertical velocity (contour, m s^{-1}) for triangle 1. (c) same as (b), but for the vertical profiles of the vorticity (shaded, 10^{-5} s^{-1}) for triangle 1.

https://doi.org/10.5194/egusphere-2024-707
Preprint. Discussion started: 15 March 2024

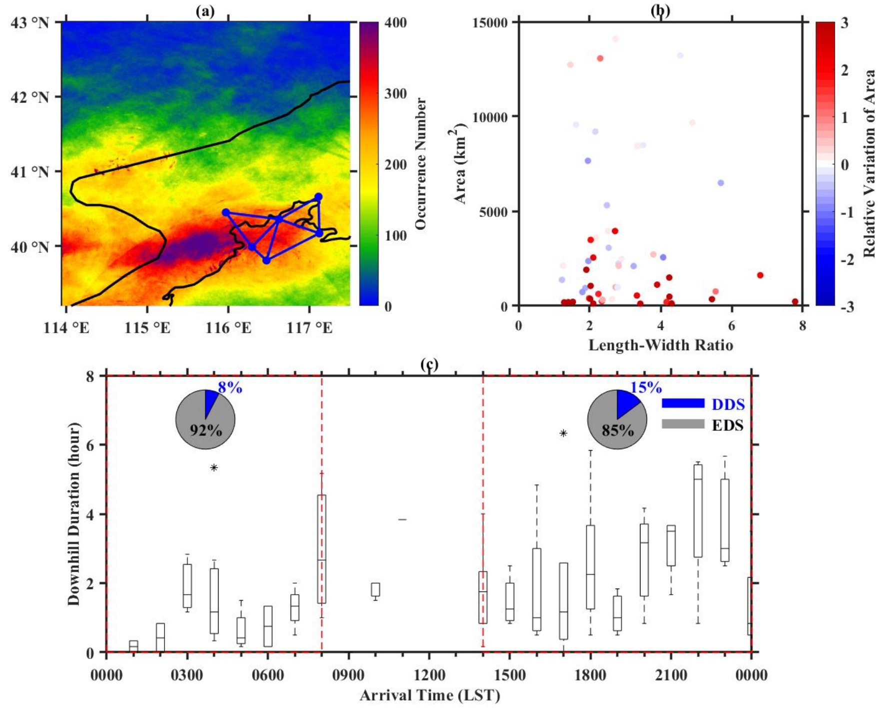

Figure 7. (a) The occurrence number (shaded) of reflectivity greater than 35 dBZ during downhill thunderstorm events. (b) Scatterplots showing the distribution of the initial length-width ratio and area of downhill thunderstorms, with the corresponding relative variation of area (shaded, km^2). (c) Boxplots showing the distribution of the arrival time and downhill duration of 96 downhill storm events. The central box represents the values from lower to upper quartile (25th–75th percentile), the vertical line extends from the 10th to 90th percentile, the solid line denotes the median. The left pie denotes the ratio of EDSs (grey) and DDSs (blue) which arrive at the plain during the period of 0100-0800 LST. The right pie denotes the same, except for during the period of 1400-0000 LST.

https://doi.org/10.5194/egusphere-2024-707
Preprint. Discussion started: 15 March 2024

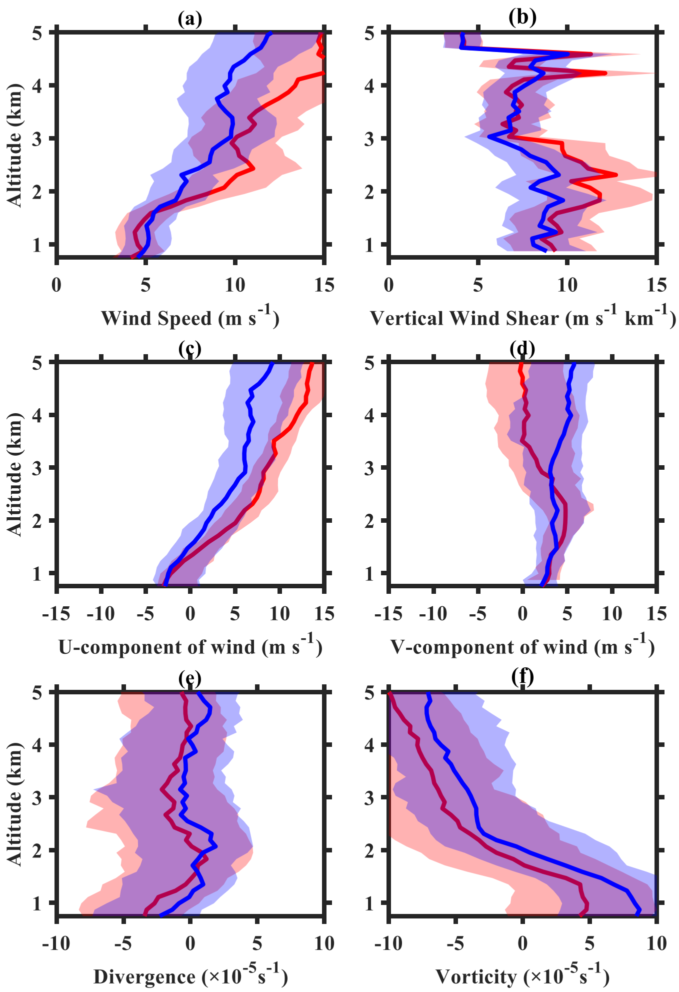

Figure 8. Vertical profiles of (a) wind speed, (b) vertical wind shear, (c) u-component of wind, (d) v-component of wind over YQ station in two hours prior to the arrival of EDSs (red) and DDSs (blue). (e) and (f) same as the above, except for the divergence and vorticity over triangle 1 as shown in Figure 1b derived from the RWP mesonet, respectively.